Journal of Inflammation Research

Dovepress
open access to scientific and medical research

Open Access Full Text Article

ORIGINAL RESEARCH

The Effect of Shaoyao Gancao Decoction on Sphincter of Oddi Dysfunction in Hypercholesterolemic Rabbits via Protecting the Enteric Nervous System–Interstitial Cells of Cajal–Smooth Muscle Cells Network

Gui-Ying Zhu*
Dan-Dan Jia*
Ying Yang
Ye Miao
Chao Wang
Chang-Miao Wang

Department of General Surgery of Integrated Traditional Chinese and Western Medicine, The First Affiliated Hospital of Dalian Medical University, Dalian, 116011, People's Republic of China

*These authors contributed equally to this work

Objective: This study observes the morphological changes in the enteric nervous system (ENS) – interstitial cells of Cajal (ICC) – smooth muscle cells (SMC) network in sphincter of Oddi dysfunction (SOD) in hypercholesterolemic rabbits following treatment with Shaoyao Gancao decoction (SGD), as well as the apoptosis of the ICC.

Methods: In this study, 48 healthy adult New Zealand rabbits are randomly divided into three groups (n = 16 in each group): the control, the model, and the SGD treatment groups. The hypercholesterolemic rabbit model is established. Hematoxylin and eosin staining, transmission electron microscopy, immunofluorescence, terminal deoxynucleotidyl transferase dUTP nick end labeling staining, immunohistochemistry, Western blot analysis, and reverse transcription-polymerase chain reaction are used to detect the morphological changes in the ENS–ICC–SMC network, the expression of apoptosis-related proteins in the ICC, and to observe the curative effect of SGD after treatment.

Results: Compared with the control group, the morphology and the ultrastructure of the SO are destroyed in the model group. In addition, the protein gene product 9.5 (PGP9.5), nitric oxide (NO), the SMCs, and the ICC all significantly decreased while substance P (SP) significantly increased. Compared with the model group, the SO morphology and ultrastructure are repaired in the SGD group. In addition, the PGP9.5, NO, the SMCs, and the ICC significantly increased while SP decreased. In addition, SGD may activate the stem cell factor (SCF)/c-Kit signaling pathway to treat SO dysfunction by up-regulating the expression of c-Kit and SCF. Similarly, this pathway restores SO by up-regulating the expression of Bcl2 and inhibiting cleaved caspase-3, Bax, and the tumor necrosis factor.

Conclusion: Shaoyao Gancao decoction can promote the recovery of sphincter of Oddi dysfunction in hypercholesterolemic rabbits by protecting the ENS–ICC–SMC network.

Keywords: sphincter of Oddi dysfunction, Shaoyao Gancao Decoction, ENS–ICC–SMC, apoptosis

Correspondence: Chang-Miao Wang
Department of General Surgery of Integrated Traditional Chinese and Western Medicine, The First Affiliated Hospital of Dalian Medical University, No. 222 Zhongshan Road, Xigang District, Dalian City, Liaoning Province, 116011, People's Republic of China
Tel +411-83635963-3145
Fax +411-83635963
Email drwangcm35@outlook.com

Introduction

Sphincter of Oddi dysfunction (SOD) is a clinical syndrome caused by abnormal contraction of the sphincter of Oddi (SO) and is an important link in the pathogenesis of most gallbladder- and pancreas-related inflammatory diseases and in

Received: 5 July 2021
Accepted: 17 August 2021
Published: 15 September 2021

functional diseases; it is also a key secondary pathological change in the context of these diseases and seriously impacts patients' quality of life.[1–3] At present, there is no effective treatment for SOD, and the research on its mechanism is in the preliminary stages. Therefore, it is urgent to study the pathogenesis of SOD to find new treatment methods.

The interstitial cells of Cajal (ICC) are non-neural interstitial cells that are vital in the regulation of gastrointestinal motility. The ICC function as information integration "transit stations" for the transmission of enteric nervous system (ENS) signals to smooth muscle cells (SMCs) and are central in controlling gastrointestinal peristalsis. Recent studies revealed that in gastrointestinal motility disorders, the number of ICC is abnormal or decreased,[4,5] or the neural transmission of the ENS–ICC–SMC network is reduced.[6,7]

The SO is a smooth muscle that has a similar smooth-muscle structure to the gastrointestinal tract and has the function of contraction and relaxation. To date, in-depth studies have been performed on the structural system of gastrointestinal smooth muscle. Therefore, studies of the smooth muscle structure of the biliary system can learn from previous gastrointestinal research. Recent research revealed that there were many ICC in the SO,[8] and the excitation of the ICC could make the SO contract preventing bile, pancreatic juice, and gastrointestinal content from entering the bile and pancreatic ducts. This result suggests that the ICC may be related to SOD.[9] The ICC, SMCs, and the ENS form a very close networked structure (the ENS–ICC–SMC network). This study speculates that the occurrence of SOD may be related to the ENS–ICC–SMC network. Shaoyao Gancao decoction (SGD) is a well-known antispasmodic traditional Chinese medicine dating back 2000 years that is widely used for the treatment of clinical spastic pain.[10,11] It also has a good therapeutic effect on SOD.[12,13] However, the principle and mechanism of the antispasmodic and analgesic effects related to SGD in the treatment of SOD have not been fully elucidated.

Based on current research of the ENS–ICC–SMC network in the gastrointestinal tract, this study speculated that the pathogenesis of SOD is related to the ENS-ICC-SMC network and that SGD may be effective in the treatment of SOD within the ENS-ICC-SMC network structure. Accordingly, in this study, the morphology and ultrastructural changes in the SO in hypercholesterolemic rabbits is observed, the morphological changes in the ENS–ICC–SMC network in the SO are explored, the expression of the apoptosis pathway and apoptosis-related proteins in the ICC of SOD model rabbits is detected, and the changes following SGD treatment are documented.

Materials and Methods

Animals

For the current study, 48 healthy New Zealand big-eared rabbits, purchased from the Laboratory Animal Center of Dalian Medical University, China (approximately 2–3 months old, weighing approximately 1.75–2.25 kg, half male and half female, with a serum total cholesterol concentration of <3.0 mmol/L), were used in this study.

The animals were raised in a standard laboratory animal environment (temperature 22°C–25°C, humidity 50–70%), and the experiment was initiated seven days following adaptive feeding. According to the random number table method, the rabbits were divided into three groups (n = 16 for each group): normal (control), model (SOD), and SGD groups. For a total of eight weeks, based on the method presented by Zhang et al,[14] the rabbits in the control group were given animal-standard rabbit feed every day, and the model group and SGD group were fed with standard rabbit feed and cholesterol (1 g of cholesterol was added to their diet six days a week, and the standard rabbit feed only was fed one day a week). According to the hypercholesterolemia model standards described in the literature, if the serum total cholesterol was >10 mmol/L, the hypercholesterolemia standard was achieved. After modeling, the rabbits in the control and model groups were given 20 mL normal saline twice daily, and rabbits in the SGD group were given 20 mL SGD twice daily. After four weeks of treatment, the rabbits were euthanized by air embolism from the marginal vein of the ear. Under aseptic conditions, the abdominal cavity was dissected along the midline of the abdomen, and the SO was separated. The obtained SO was divided into two parts, one of which was placed in a liquid nitrogen tank and transferred to a −80°C refrigerator for storage. The second part was fixed in 4% paraformaldehyde or 2.5% glutaraldehyde and stored in a 4°C refrigerator for use in the subsequent experiment. The study was conducted in strict accordance with the recommendations of the National Institutes of Health Guidelines for the Care and Use of Laboratory Animals. All animal experimental procedures were approved by the Animal Care and Use Committee at Dalian Medical University [SCXK(Liao)

2018-0003] and complied with the principle for replacement, refinement, or reduction.

Preparation of the Shaoyao Gancao Decoction

According to the dosage of Zhang Zhongjing's Treatise on Febrile Diseases, Shaoyao and Gancao (Beijing Tongrentang, Dalian Branch, China) were converted into a modern dosage. The ratio of Shaoyao and Gancao was 1:1 (62.5 g each). The dose was calculated according to the proportion of SGD (125 g) used in adults (60 kg). The equivalent effective dose for a rabbit was calculated as follows: 3.7 (conversion coefficient) × 125 g/60 kg ≈ 8 g/kg. According to the previous experiment, a double dose of SGD resulted in a good clinical effect, so a dosage of 16 g/kg was selected for this study. After soaking the two drugs together for approximately 30 min, they were decocted three times. The first time, 10 times water was added, and 8 times water was added the second and third time (1 h decoction time for each). The SGD was obtained three times, after which the three obtained decoction solutions were mixed. The final SGD was concentrated using a rotary evaporator. The active components of the crude drug were approximately 2.4 g×ML^{-1}; the SGD was administered by gavage (20 mL each time, twice daily, six days a week, 28 days in total).

Hematoxylin and Eosin Staining

The obtained SOs were fixed in 4% paraformaldehyde overnight. Concentration gradient alcohol was used to achieve dehydration, after which they were treated with xylene for 30 min. The tissue blocks were then placed in containers containing xylene and paraffin and stored in a temperature box at 60°C for approximately 2 h to ensure the paraffin completely penetrated the tissue. The dissolved wax was poured into the metal frame, the tissue was buried at the center of the metal frame, and a wax block finally formed. The wax block was placed on a paraffin microtome and cut into 5-μm thick sections. The sections were subsequently unfolded in a warm water pan. The unfolded tissue sections were transferred to a slide, placed in an oven, and dried at 60°C for 4 h. Before staining, the sections were immersed in xylene I and xylene II for approximately 15 min each. The slices were then submerged in absolute ethanol I and absolute ethanol II where they soaked for approximately 5 min. Then, the dehydrated sections were immersed in different levels of ethanol (95%, 85%, and 75%). The sections were soaked in each level of ethanol for approximately 2 min, and then stained with hematoxylin and eosin (H&E). The slices were put into hematoxylin and then soaked in distilled water for about 5 min each. Next, the slices were placed in 1% hydrochloric acid alcohol, reacted for about 3 s, then rinsed in running water for 20 min. They were then immersed in distilled water for 2 min. Finally, the slices were immersed in eosin solution for 3 min. After staining, the slices were immersed in concentration gradient ethanol (75%, 85%, and 95%). The residence time at each level was approximately 2 min. Next, the slices were immersed in absolute ethanol I and II where they were soaked for about 5 min each. After dehydrating the slices in xylene, I and xylene II, where they soaked for about 10 min, the slices were sealed with neutral resin glue.

Transmission Electron Microscopy

The SOs were fixed in 2.5% glutaraldehyde at 4°C for 2–4 h and rinsed three times with a 0.1 M phosphate buffer saline (PBS; pH 7.4, 15 min each time). The specimens were fixed in 1% osmium acid solution, dehydrated in graded alcohol, and embedded in Eponate 812 resin. Next, 3-μm sections were stored at 4°C for 2 h. Tissues were cut and stained with 2% toluidine blue to highlight the cellular structure. After visually identifying sections containing characteristic structures, ultrathin sections were obtained with a Leica UC7 ultra-microtome. Thin sections were collected on 200 mesh grids, stained with 2% uranyl acetate for 15 min and lead citrate for 5 min, and observed by transmission electron microscopy (TEM).

Immunofluorescence Staining

Immunofluorescence Single Staining

Paraffin-embedded sections were dewaxed in water, xylene, and gradient ethanol, placed in the antigen recovery solution, heated in a microwave oven to recover the antigen, cooled to room temperature, and treated with a 0.5% Triton X-100 solution for 5 min. The non-specific binding sites were blocked with 5% bovine serum albumin (BSA) for 1 h at room temperature. Protein gene product (PGP) 9.5 and α-actin (see Table 1) were left standing in a damp dark room at 4°C overnight and added to the sections that were washed with PBS and incubated as secondary antibodies at 37°C for 60 min in the dark.

Immunofluorescence Double Staining

The nitric oxide synthase (nNOS) and substance P (SP) antibody mixture (Table 1) was diluted in proper

Table 1 Antibodies Used in the Experiment

Description	Company
PGP9.5	Affinity Company
α-action	Abcam Company
nNOS	Abcam Company
c-kit antibodies	Bioss Company (China)
Substance P	Affinity Company
TUNEL kit	Servicebio Company
Cleaved Caspase3	Wanleibio Company (China)
Bcl2	Wanleibio Company (China)
Bax	Wanleibio Company (China)
β-Actin	Wanleibio Company (China)

proportion and added to the tissue for overnight incubation at the same time. Diluted and mixed secondary antibodies (Cy3 labeled goat anti-rabbit IgG and FITC-labeled goat anti-mouse IgG) were added for incubation. The remaining steps were the same as in single staining.

Terminal Deoxynucleotidyl Transferase dUTP Nick End Labeling Immunofluorescence Staining

Terminal deoxynucleotidyl transferase dUTP nick end labeling (TUNEL) immunofluorescence staining was used to detect apoptotic cells, and immunofluorescence for the c-kit antibody was utilized to locate the ICC. The paraffin-embedded sections were treated with a 0.5% Triton X-100 solution for 5 min, and the nonspecific binding sites were blocked with 5% BSA for 1 h at room temperature. The c-kit antibody (Table 1) was added to the sections and incubated overnight in a damp dark room at 4°C. After washing with PBS, the tissue blocks were incubated with secondary antibodies at room temperature for 2 h. A TUNEL apoptosis assay kit (Roche Diagnostics, Switzerland) was used for staining according to the manufacturer's instructions. After washing with PBS, the sections were examined under a fluorescence microscope (Olympus, Tokyo, Japan). The Image-Pro Plus 6.0 software program was used to conduct an optical density quantitative analysis, and the average optical density was read.

Immunohistochemical Staining

Immunohistochemistry was performed to detect apoptosis-related proteins, such as cleaved caspase-3, Bax, and Bcl-2. Paraffin-embedded sections were dewaxed in water, xylene, and gradient ethanol, placed in the antigen recovery solution, heated in a microwave oven to recover the antigen, then cooled to room temperature. The sections were placed in a 3% H_2O_2 solution and incubated at room temperature for 15 min to eliminate the endogenous peroxidase activity, and the non-specific binding sites were blocked by 5% BSA at room temperature for 60 min. Cleaved caspase-3, Bax, and Bcl-2 primary antibodies were added to the sections and incubated overnight in a humidified dark room at 4°C. This was followed by incubation of the appropriate secondary antibodies. Subsequently, the sections were stained with 3,3-diaminobenzidine (DAB) solution and counterstained with hematoxylin. Negative controls were prepared by omitting primary antibodies to check the specificity of the immunostaining.

Western Blot

Per the instructions of the total protein extraction kit (Wanleibio), cleavage was performed, and protein lysates were extracted from the SO tissue to detect the expression levels of protein. The protein concentrations were measured using a BCA protein assay kit (Wanleibio). Samples were run on SDS-polyacrylamide gel electrophoresis and transferred onto PVDF membranes. The membranes were incubated in 5% milk to reduce the non-specific binding. Antibodies against c-kit, the cleaved caspase-3, Bax, and Bcl-2 antibodies, and β-actin (1:1000 dilution) were used for Western blotting. The first antibody was placed in a damp dark room at 4°C overnight and subsequently added to the sections. After washing with PBS, the membranes were incubated with the secondary antibody (HRP-labeled goat anti-rabbit IgG; 1:5000) for 2 h at room temperature and were processed for exposure. The densities of the bands were quantified using protein assay software (Bio-Rad Co, CA, USA). All primary antibodies utilized in this study are listed in Table 1.

Real-Time Quantitative Polymerase Chain Reaction

Total RNA was extracted from the SO using a TRI pure reagent (BioTeke, Beijing, China). Then, a super M-MLV reverse transcriptase kit (BioTeke), RNase inhibitor (BioTeke), and Taq polymerase chain reaction (PCR) MasterMix (2X) (BioTeke) were used to transform RNA into cDNA. The fluorescence quantitative analysis was performed using an Exicycler TM 96 fluorescence quantitative instrument (BioNeer, the Republic of Korea). All PCR amplifications were repeated three times. The transcription level was normalized to the β-Actin level. Table 2 presents the specific primers and probes of stem cell factor (SCF), tumor necrosis factor (TNF)-α, and β-

Table 2 Primer Sequences

Primer Sequence Name	Sequence
TNF-α F	AGGAGGAAGAGTCCCCAA
TNF-α R	TTGCGGGTTTGCTACTACG
SCF F	ACCCAGACCCTTTACTCCT
SCF R	TGGAACTTTCAGCCTTGC
β-actin F	CCAGGTCATCACCATCGG
β-actin R	TGTCCACGTCGCACTTCA

actin. The $2^{-\Delta\Delta CT}$ method was used to quantify the relative changes in gene expression.

Statistical Analysis

All data were expressed as the mean ± standard deviation. A one-way analysis of variance (ANOVA) was conducted using the SPSS 24.0 (SPSS, Chicago, USA) software program in all tests, and a *P* value of 0.05 was considered statistically significant. Prism 5.0 software (GraphPad, San Diego, USA) plotted all data.

Results

Animal Model Assessment

The hypercholesterolemic rabbit model is the only reliable SOD model.[15] This study's research team successfully reproduced this model. When the serum cholesterol of rabbits was >10 mmol/L, the SOD was considered to have been successfully induced.[14,16] This modeling method has been repeatedly verified by other research teams. In this study, the serum cholesterol levels of the model and treatment groups were significantly higher than 10 mmol/L after providing a high cholesterol diet, while the serum total cholesterol in the control group were lower than 3 mmol/L (Figure 1).

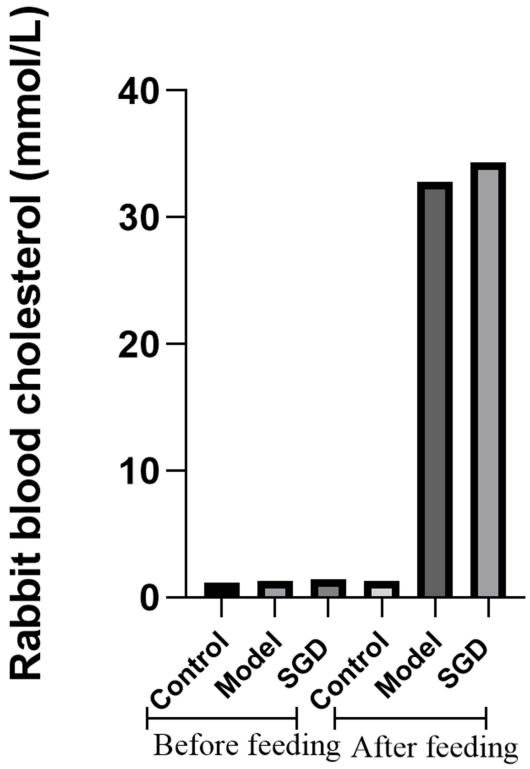

Figure 1 Serum total cholesterol concentration of the rabbits before and after modeling.

Observation of the Sphincter of Oddi Pathophysiology

Hematoxylin and Eosin Staining Observation

The H&E staining showed that the inflammation in the model group was relatively severe. Specifically, in the control group, the SO structure was clear, the mucosal epithelial cells were intact, and the lamina propria of the mucosa was accompanied by scattered inflammatory cell infiltration (a relatively normal finding). In the model group, the SO structure was partially damaged, the mucosal epithelial cells were lost, the fibrous tissue of the lamina propria of the mucosa was loose and showed edema, and the mucous layer was accompanied by a large amount of inflammatory cell infiltration. However,in the SGD group, the structure of the SO was also partially destroyed, the mucosal epithelial cells were incomplete, and the lamina propria of the mucosa demonstrated fibrous tissue proliferation accompanied by inflammatory cell infiltration that was relatively mild compared with the model group (as is shown in Figure 2).

Detection of the Sphincter of Oddi by Transmission Electron Microscopy

When viewed under an electron microscope, in the normal group, the nuclei of the ICC were large (accounting for the majority), had less cytoplasm, and rich organelles were closely connected with the surrounding cells and nerve fiber ends. In the model group, the ICC were severely swollen, the cell membrane was intact, and the surrounding collagen fibers (CFs) were sparse. In addition, a large part of the low electron density edema area had been dissolved, the nucleus was irregular, the chromatin was sparse, the nuclear membrane was fuzzy, and the nucleolus (Nu) was small. The mitochondria were observably swollen, the membrane matrix was dissolved, the wave crest was broken and decreased, and the membrane was seriously damaged and decomposed. The rough endoplasmic reticulum (RER) was significantly expanded, threshed, and vacuolated. The number and distribution of the dense

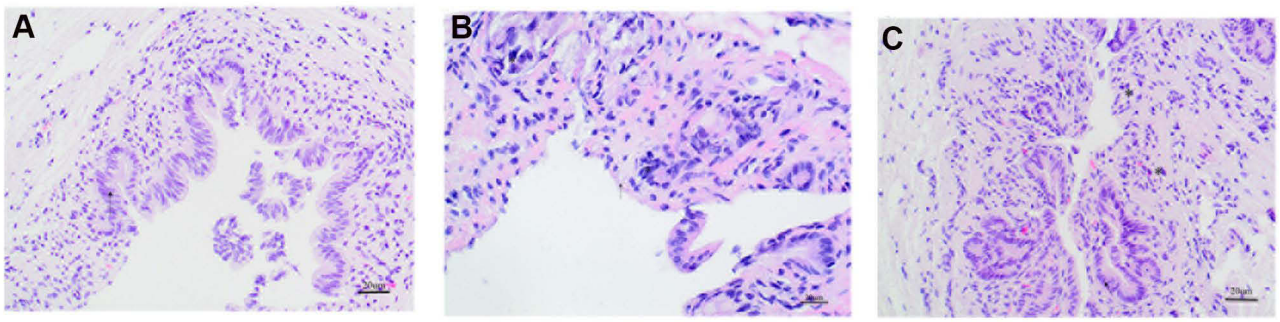

Figure 2 Hematoxylin and eosin staining of rabbit SO tissue (400×, 20 um), (**A**) Normal group, (**B**) Model group, (**C**) Treatment group. The arrow (←) refers to mucosal epithelial cells, the (*) refers to inflammatory cells infiltration.

points (DPs) and dense bodies (DBs) in the SMCs were less and uneven, respectively, and the sizes of the DPs were not uniform and were irregularly shaped. In the SGD group, the ICC were spindle-shaped, contracted, and slightly swollen. The cell membrane was intact, a large number of CFs were evenly distributed, the nucleus was irregular, the Nu was at the center, and the heterochromatin was clustered. The mitochondrial membrane was intact, and the membrane matrix was lighter. The RER was slightly expanded, and the DPs and DBs were evenly distributed. In addition, the size of the dense area was uniform. In general, the SO injury in the model group was the most serious, followed by the injury in the SGD group, and the normal group was relatively normal (Figure 3).

Detection of Nerve Fibers and Smooth Muscle Cells

Immunofluorescence microscopy revealed that integrated option density (IOD) values ofthe PGP9.5 and α-action were significantly lower in the model group compared with the control group. In the treatment group, these values were observed as being between those in the remaining two groups (model group < treatment group < control group). There were significant differences among the three groups ($P < 0.05$; see Figure 4). Immunofluorescence double staining of nNOS and SP, nNOS specifically labeled nitric oxide (NO), and the IOD value of nNOS were the highest in the control group and the lowest in the model group. The IOD value of SP was the lowest in the control group and highest in the model group ($P < 0.05$). The level of excitatory neurotransmitter SP represented the increase of SO-induced contraction, and the level of inhibitory NO represented the relaxation degree of the SO. These values indicated that the contraction degree of the SO was greater in the model group than in the treatment and control groups, and the relaxation degree of the SO was lower in the model group than in the control group. Compared with the model group, NO increased and SP decreased. This suggested that NO in the SGD group could promote the release of NO and inhibit the release of SP (Figure 5).

Detection of Interstitial Cells of Cajal Apoptosis

In this study, the number of positive cells and double-positive cells in the cross-section of the ICC were calculated. In normal SO tissue, most of the ICC positive cells were distributed in the muscle layer and had a long fusiform-to-oval shape. There were a smaller number of ICC positive cells in the model group compared with the control group ($P < 0.05$). The number

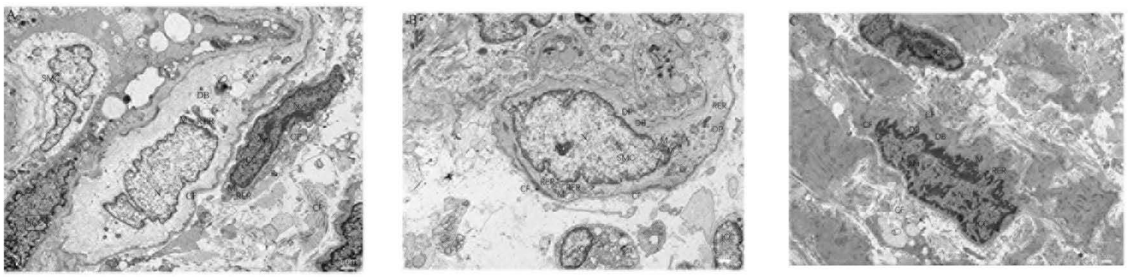

Figure 3 Rabbit SO tissue electron microscopy (1.0 um), (**A**) Normal group, (**B**) Model group, (**C**) Treatment group. The definitions of the abbreviations in the picture are as follows: interstitial cells of Cajal (ICC), smooth muscle cells (SMC), nucleus (N), nucleolus (Nu), mitochondria (M), rough endoplasmic reticulum (RER), collagen fibers (CF), dense spots (DPs), and dense bodies (DBs).

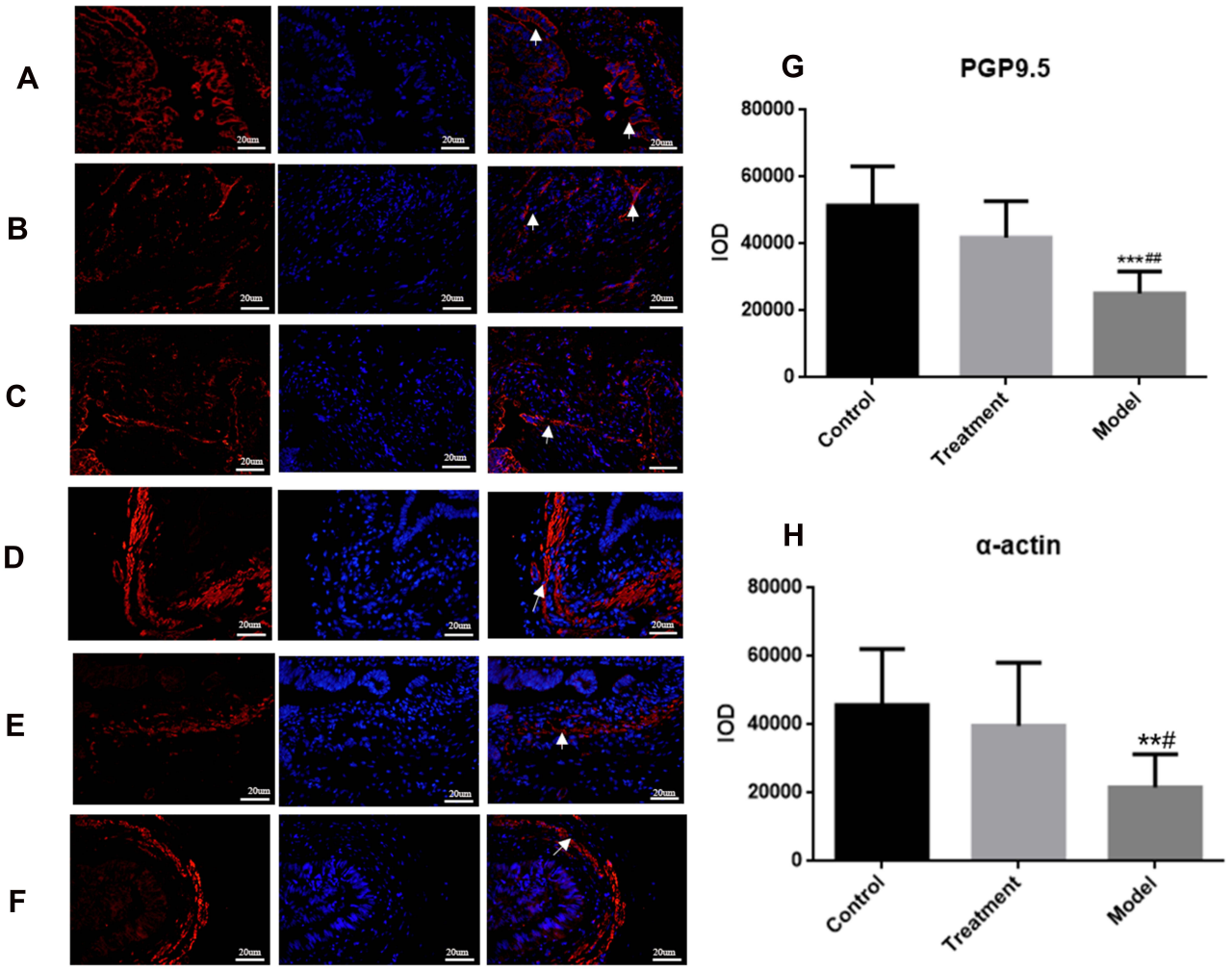

Figure 4 (**A**) Normal group, (**B**) Model group, (**C**) Treatment group: Rabbit SO tissue, nerve fiber PGP9.5 in the inner muscular layer detected by laser confocal microscopy, red light is PGP9.5, blue light is DAPI. (**D**) Normal group, (**E**) Model group, (**F**) SGD treatment group: α-actin labeled rabbit SO tissues were examined by laser confocal microscopy (400×, 20 um), with α-actin in red light and DAPI in blue light. (**G**) fluorescence intensity of PGP9.5 (IOD) in the SO tissue of rabbits in each group; (**H**) The fluorescence intensity (IOD) of α-actin labeled SMC in the SO tissue of rabbits in each group. Arrows indicate positive expression.*** indicates the comparison between the model group and the control group, P<0.05, ##indicates the comparison between the model group and the treatment group, P<0.05. In α-action, ** indicates the comparison between the model group and the control group, P<0.05, # indicates the comparison between the model group and the treatment group, P<0.05.

of ICC positive cells increased in the SGD group, and the difference was statistically significant. The ratio of double-positive cells to ICC positive cells showed the apoptosis rate of the ICC. The results revealed that the apoptosis rate of the ICC increased in the model group compared with the control group ($P < 0.01$). However, the proportion in the SGD group significantly decreased compared with the model group ($P < 0.05$; see Figure 6).

Detection of the Apoptosis Pathway of Caspase-3/Bax/Bcl-2 in Interstitial Cells of Cajal

Caspase-3 is an effector protease located downstream of the caspase family and is a very critical protein in the process of apoptosis. The Bcl2 family can promote or inhibit apoptosis. Both Bcl2 and Bax are important members of the Bcl2 family. Bcl2 has the effect of inhibiting apoptosis, and Bax has the effect of promoting apoptosis. In this study, the expression of cleaved caspase-3, Bax, and Bcl-2 in the SOs was detected by immunohistochemistry. The results in the model group revealed that, compared with the control group, the average optical density of cleaved caspase-3 and Bax increased while that of Bcl-2 decreased ($P < 0.05$). In the SGD group, compared with the model group, the average optical density of cleaved caspase-3 and Bax decreased while that of Bcl-2 increased ($P < 0.05$; see Figure 7). Western blot analysis was performed to detect the expression levels of c-kit, cleaved caspase-3, Bax,

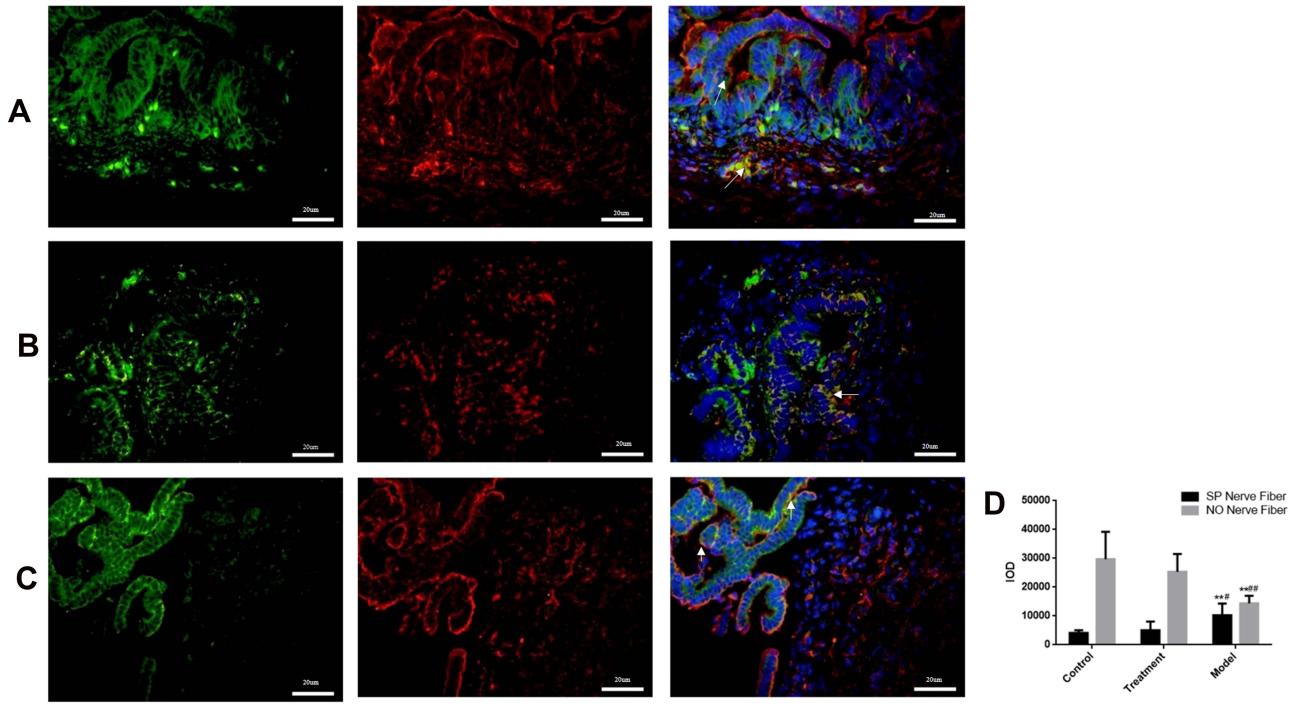

Figure 5 (**A**) Normal group, (**B**) Model group, (**C**) Treatment group: Rabbit SO tissue, nerve fiber in the inner muscular layer detected by laser confocal microscopy, SP and n-NOS respectively labeled SP nerve fibers (green light) and NO nerve fibers (red light) in rabbit SO tissue. The blue light is DAPI. Arrows indicate positive expression. ** indicates that the model group is compared with the control group, $p<0.05$, # indicates that the model group is compared with SGD group,$p<0.05$.In NO, ** indicates that the model group is compared with the control group, $p<0.05$, ## indicates that the model group is compared with SGD group, $p<0.05$.

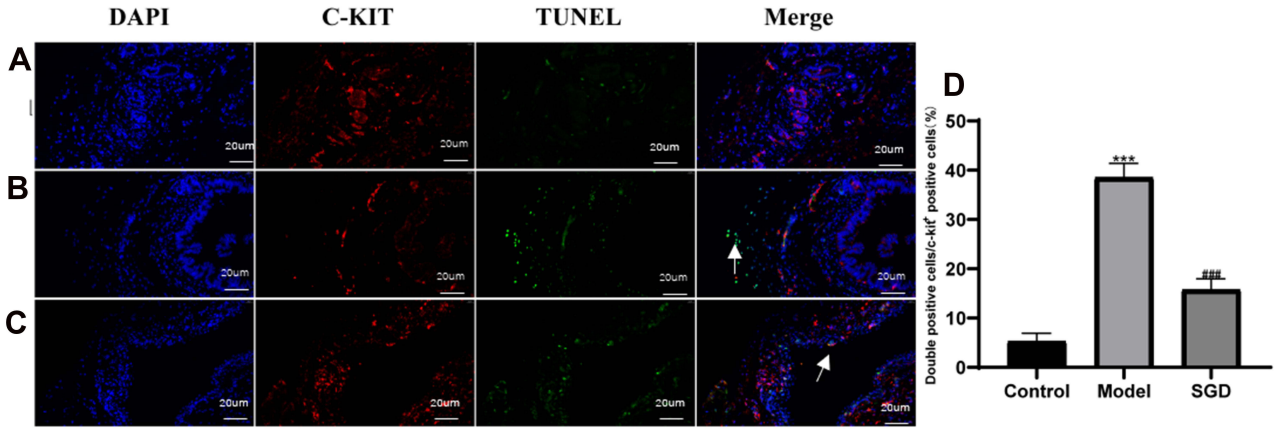

Figure 6 Results of ICC and TUNEL fluorescence staining in the SO tissue of rabbits (400×, 20 um); Blue is DAPI staining, red is c-kit positive ICC cell staining, green is TUNEL apoptotic cell staining. (**A**) Normal group, (**B**) Model group, (**C**) Treatment group, (**D**) ICC double positive expression rate. The model group vs the control group, ***$P \leq 0.001$. The SGD group vs the model group, ###$P \leq 0.001$. Arrows indicate positive expression.

and Bcl-2 in the SO tissue of the control, model, and SGD groups. The results reveal that the expression of cleaved caspase-3 and Bax protein significantly increased in the model group ($P \leq 0.001$ for all) compared with the control group, and the expression of c-kit and Bcl-2 protein significantly decreased in the model group ($P < 0.001$ for all). Compared with the model group, the expression of cleaved caspase-3 and Bax protein in the SO tissue of the SGD group significantly decreased ($P < 0.01$) while the expressions of c-kit and Bcl-2 protein in the SO tissue of the SGD group significantly increased (all $P < 0.05$; see Figure 8).

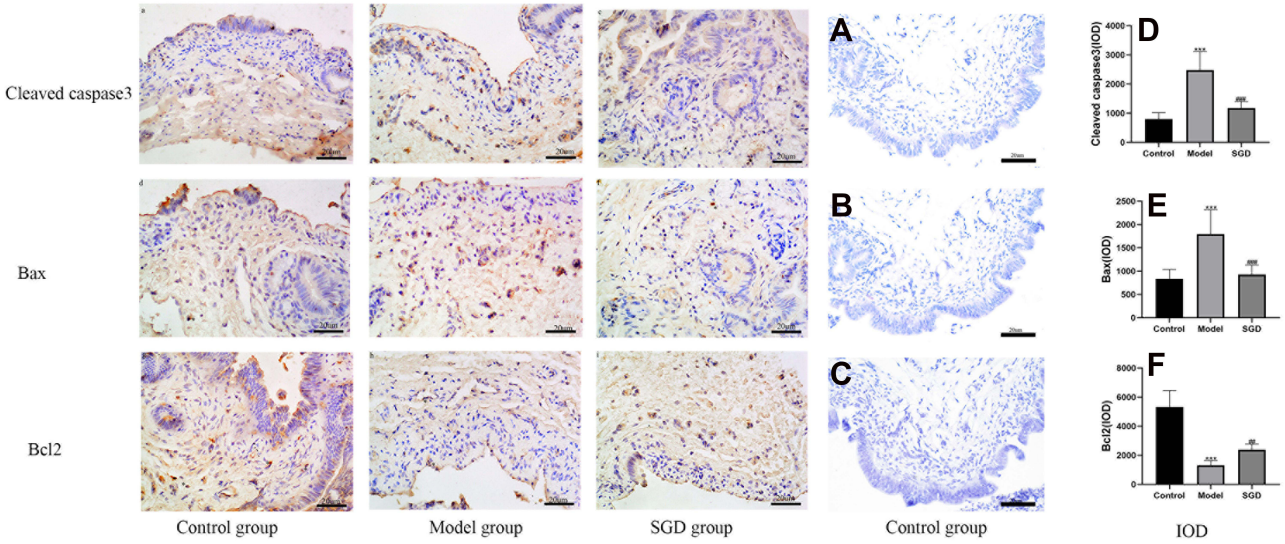

Figure 7 Immunohistochemical results of cleaved caspase-3, Bax, and Bcl2 in SO tissue (400×); a, b, and c: cleaved caspase-3 immunohistochemical results in the normal group, model group, and SGD treatment group, respectively; d, e, and f: Bax immunohistochemical results in the normal group, model group, and treatment group, respectively; g, h, and i: Bcl2 immunohistochemical results of the normal group, the model group, and the treatment group, respectively. The brown or brown cytoplasm is the expression of the corresponding positive protein (*). (**A**–**C**) The negative controls for cleaved caspase-3, Bax, and Bcl2 using control samples, respectively. (**D**–**F**) Respectively fluoresced caspase-3, Bax, and Bcl2 (IOD) in the SO tissue of rabbits in each group. The model group vs the control group, ***P ≤ 0.001. The SGD group vs the model group,###P≤0.01, ####P ≤ 0.001.

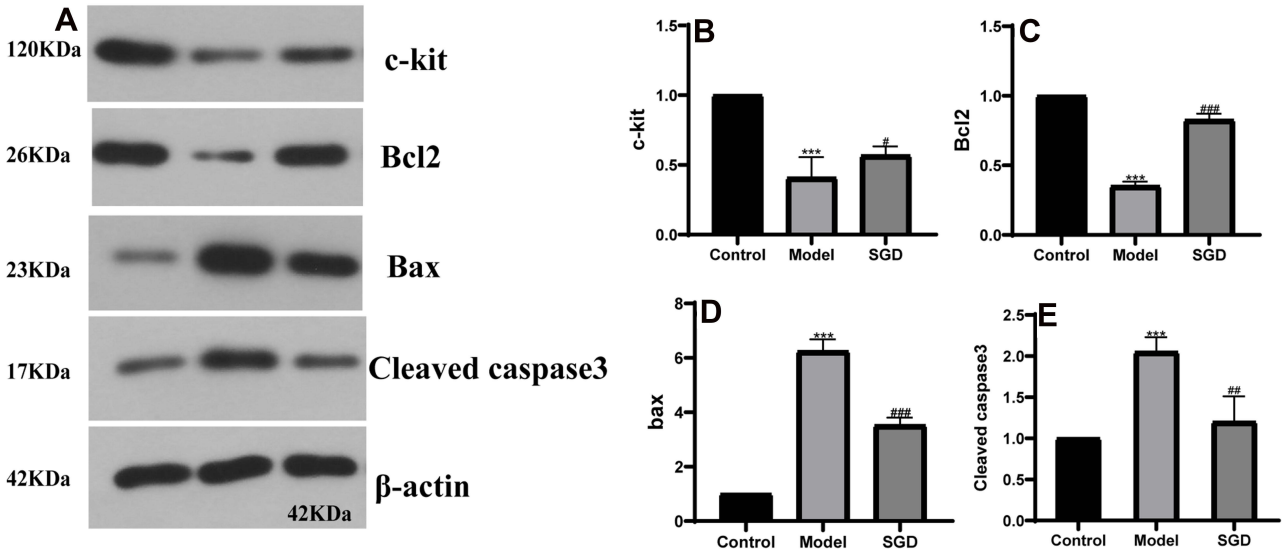

Figure 8 (**A**) the protein band; (**B**–**E**) the protein results of c-kit, Bcl2, Bax, and cleaved caspase-3 in rabbit SO tissue, respectively. The model group vs the control group, ***P ≤ 0.001, the SGD group vs the model group, #P ≤ 0.05, ##P ≤ 0.01, ###P ≤ 0.001.

Detection of the Stem Cell Factor/c-Kit Signaling Pathway and Tumor Necrosis Factor-α Pathway

The SCF is often used as a natural ligand for the c-kit receptor, and the tumor necrosis factor (TNF-α) is generally considered a pro-inflammatory cytokine and apoptosis-inducing factor. Compared with the control group, the expression of SCF mRNA significantly decreased in the model group (P < 0.001). Compared with the model group, the expression of SCF mRNA increased in the SO tissue of the SGD group (P < 0.001). The expression of the TNF-α mRNA significantly increased in the model group (P < 0.01) compared with the control group. Compared with the model group, the expression of TNF-α mRNA in the SO

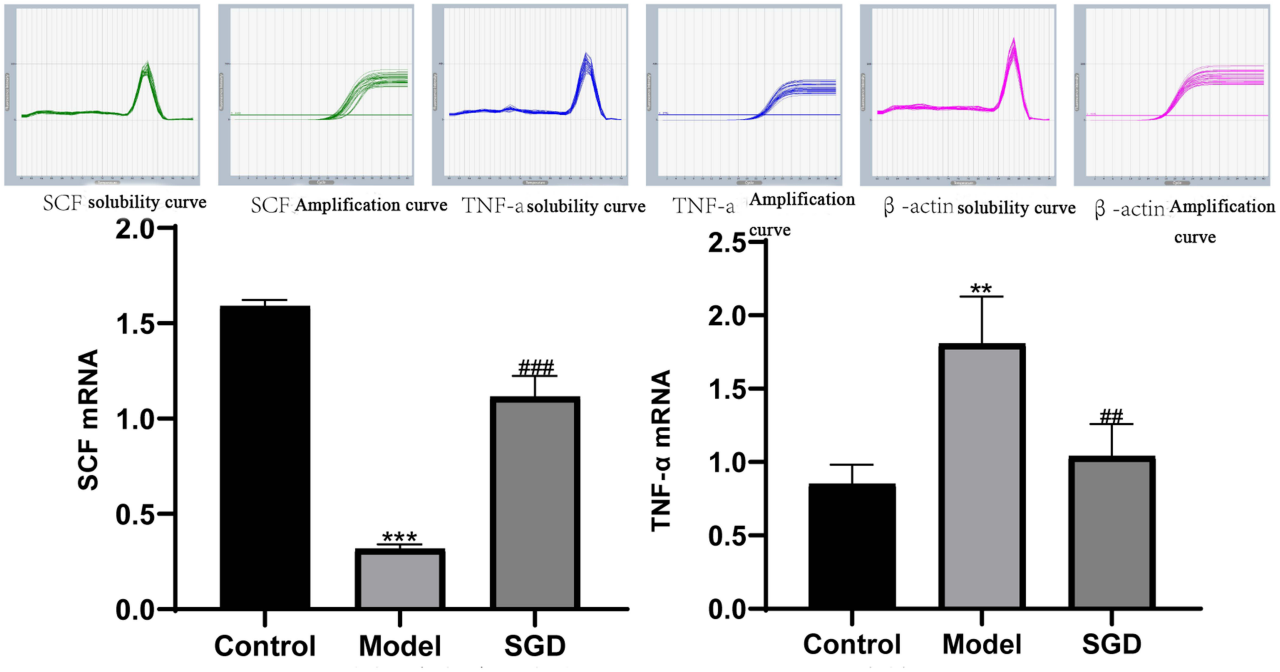

Figure 9 (**A** and **B**) the results of SCF and TNF-α mRNA in the SO tissue of rabbits in each group. The control group vs the model group, **P ≤ 0.01, ***P ≤ 0.001. The SGD group vs the model group ##P ≤ 0.01, ####P = 0.001 or less.

tissue of the SGD group significantly decreased (P < 0.01; Figure 9).

Discussion

The SO is an important structure located at the junction of the biliopancreatography and the duodenum and not only regulates the excretion of bile and pancreatic juice but also controls the anti-reflux effect.[17,18] High cholesterol can lead to SOD in rabbits. Szilvassy et al[19,20] first reported hypercholesterolemia and hypertriglyceridemia with SOD. In 2000, Wei et al[16] successfully established a rabbit SOD model by feeding cholesterol to New Zealand rabbits; the researchers found that high cholesterol level induced SOD in rabbits. In addition, the SO in rabbits is exposed to the duodenal wall, so it is a good animal to study.[21]

Herbal medicines have always been an important resource for the discovery of candidate drugs.[22,23] The SGD originated from Zhongjing Zhang's Treatise on Febrile Diseases. SGD is a commonly used compound preparation comprising a 1:1 ratio of Shaoyao and Gancao and is used for the treatment of pain-related diseases. Researchers have discovered that SGD reduces muscle tension, relieves spasms, and provides analgesia.[24,25] Multiple studies have verified that Shaoyao and Gancao have antispasmodic and smooth-muscle relaxation effects and can act synergistically when used together.[26–28] Existing studies conducted by the research team also confirmed that paeoniflorin, an extract of Shaoyao, and SGD can relax the muscle rings of hypercholesterolemic rabbits.[29,30] Additionally, SGD is very effective at treating SOD in clinical practice.[12] In the present study, the histological structure of the SO and the cellular structure of ICC were observed by H&E staining and TEM. SGD administration demonstrated the ability to repair the structure and ultrastructure of the SO to different degrees.

The motor activity of the SO is involved in a variety of regulatory mechanisms including intestinal nerve activity, smooth muscle contraction function, and the ICC.[31] Existing research revealed a special functional relationship of the ENS–ICC–SMC network in the form of a synaptic connection between the ENS and the ICC[32] and a gap junction between the ICC and the SMCs,[33] resulting in the formation of a complete functional structure that is important in gastrointestinal motility.[34,35] Studying this network is important in the search for effective treatment methods for SOD. The ICC are considered "information integration transit stations" for the transmission of ENS signals to the SMCs. The ICC are also primary target cells of multiple different types of nerve fibers that include different types of receptors on their surface. In addition, SP and nNOS are closely related to the ICC, providing

evidence for the role of the ICC in nerve signal transmission and regulation.[7,36]

NO is an autocrine and paracrine signaling pathway molecule that can inhibit smooth muscle contraction. The introduction of NO to the intestinal nervous system as an inhibitory neurotransmitter has been important research progress.[37] Studies have found that the ICC play an important role in NO signaling transmission.[38] In selected inflammatory bowel diseases, the ICC were seriously damaged, and the gastrointestinal tract was highly expanded, resulting in the absence of electrical activity.[39] SP is a member of the tachykinin family and primarily exists in the efferent neurons of the ENS; it is released by excitatory neurons and acts as an excitatory neurotransmitter that can enhance the contraction of intestinal smooth muscle and promote intestinal movement. NO and SP have relational regulatory roles in the gastrointestinal tract and function in a coordinative and cooperative manner.[40] The present study revealed that, compared with the control group, the IOD value of SP in the SO tissue of the model group significantly increased, and the expression of NO in the model group significantly decreased. It is speculated that the excitatory neurons were activated when the SO was continuously stimulated by damage. Continuous activation produces impulse and release SP to enhance sphincter contraction, promotes the activity of immune cells, coordinates the migration of immune cells, and results in the inhibition of the release of NO (an inhibitory neurotransmitter), leading to SOD. Following a period of SGD treatment, the NO inhibitory neurotransmitter will increase, and the SP excitatory neurotransmitter will decrease. This will result in different degrees of repair of the nerve fibers and smooth muscle. It is speculated that during the occurrence and development of SOD and the treatment with SGD, NO and SP have important functions. However, a relevant experiment revealed that expressions of nNOS and SP decreased in patients with gastric stromal ICC deficiency and type 2 diabetes mellitus.[41] Therefore, the exact mechanism in this regard is unclear and requires more research.

In the present study, immunofluorescence staining was performed for PGP9.5 and SMCs (α-action). The results revealed that compared with the control group, the expression of PGP9.5 in nerve fibers and SMCs in the SO tissue of the SOD model rabbits significantly decreased. Following a period of SGD treatment, the expression of PGP9.5 in nerve fibers and SMCs was increased. It is speculated that the occurrence of SOD disease led to a decrease in the number of nerve fibers and SMCs, and that SGD can protect nerve fibers and SMCs. However, the results of an existing study[42] also revealed that, in the acute stage of diabetes, intestinal neurogliocytes could protect intestinal epithelial neurons from injury by releasing various nutritional factors and safeguard the expression of PGP9.5 without significant change. As an important component of the ENS–ICC–SMC pathway, the activity and expression of neurons are affected by many factors. Understanding the role of nerves in the SOD process remains a significant challenge. As such, additional focus and discussion should be given to the ENS in future experiments.

Past research has indicated that gastrointestinal injury may lead to a decrease in the number of the ICC. ICC loss has been associated with slow transit constipation, chronic idiopathic intestinal obstruction, diabetes, and other human dyskinesia.[43–46] The mitochondrial pathway is considered to be the most important pathway of apoptosis. In a pathological state, the permeability of the mitochondria increases, and cytokines are released, promoting apoptosis. This activates caspase-3, the primary executor of apoptosis. However, the activation of caspase is strictly controlled by the Bcl-2 family of proteins[47] that can be divided into anti-apoptotic and pro-apoptotic Bcl-2 proteins. Bcl-2 can inhibit apoptosis while Bax can activate apoptosis.[48] TNF-α is an inflammatory cytokine that is responsible for various signaling events in cells, leading to necrosis or apoptosis.[49] The SCF/c-kit receptor tyrosine kinase signaling pathway plays a key role in the regulation of cell development in various mammalian organs. The ICC depend on the expression of the c-kit–SCF signal to maintain their phenotype;[50,51] destruction of the SCF/c-kit signaling pathway will lead to the failure of the ICC and abnormal electromechanical coupling.[52]

In the present study, the effect of SGD on the apoptosis of the ICC in the SO of hypercholesterolemic rabbits and its related mechanisms were studied. The markers selected in this study are widely considered indicators and methods of ICC apoptosis detection.[53] Through a variety of experimental techniques, ICC apoptosis was found not only as the pathogenesis of SOD but also had a key link with SGD in SOD treatment. The results of TUNEL and c-kit immunofluorescence double staining revealed that in the model group, the number of the ICC was the largest, and the apoptosis rate was the highest. This was followed by the SGD group, and the lowest rate was found in the normal control group. The results of immunohistochemistry,

Western blot analysis, TUNEL, and c-kit double staining also confirmed that in the model group, the number of apoptotic ICC increased, and the expression of cleaved caspase-3 and Bax protein was higher than in the SGD and control groups. In the SGD group, the number of apoptotic ICC and the expression levels of cleaved caspase-3 and Bax protein were smaller and lower than in the model group but larger and higher than in the control group. The expression of Bcl-2 was the highest in the control group, and higher than in the SGD and model groups. To determine the overall expressions of SCF and TNF-α in the SO, real-time PCR was performed. The present study also revealed that in the model group, the expression of SCF mRNA significantly decreased. Following SGD treatment, SCF mRNA increased, suggesting that the blocking of the SCF/c-kit signaling pathway may be related to the consumption of the ICC in SOD. After blocking the SCF/c-kit signaling pathway, SGD was able to promote the recovery of the ICC. Other experimental data also confirmed that dysfunction in the SCF/c-kit signal transduction may serve as a basis for the decline in the number of ICC and their network function in diseases. In the model group, the expression of TNF-α mRNA was significantly higher compared with the control group. Following SGD treatment, the TNF-α in SOD rabbits decreased. These results suggest that TNF-α is also involved in the development of SOD and the mechanism of SGD treatment.

Conclusion

This study's results suggest that the occurrence and development of SOD are closely related to the ENS–ICC–SMC network in the SO. After a period of SGD treatment, the number of ICC increased and the apoptosis rate of the ICC significantly decreased when compared with SOD rabbits, suggesting that SGD may protect the ICC (by inhibiting ICC apoptosis) and may regulate the movement of the SO by affecting the ICC. These observations will contribute to the development of new therapeutic strategies. However, the regulation and apoptosis mechanisms in the ENS–ICC–SMC network are extremely complex. Experimental and clinical studies are needed to support this view.

Funding

National Natural Science Foundation of China (No.81774082).

Disclosure

The authors report no conflicts of interest in this work.

References

1. Leung WD, Sherman S. Endoscopic approach to the patient with motility disorders of the bile duct and sphincter of Oddi. *Gastrointest Endosc Clin N Am*. 2013;23(2):405–434. doi:10.1016/j.giec.2012.12.006
2. Crittenden JP, Dattilo JB. *StatPearls (StatPearls Publishing Copyright © 2021*. StatPearls Publishing LLC.; 2021.
3. Behar J, Corazziari E, Guelrud M, Hogan W, Sherman S, Toouli J. Functional gallbladder and sphincter of oddi disorders. *Gastroenterology*. 2006;130(5):1498–1509. doi:10.1053/j.gastro.2005.11.063
4. Takayama I, Daigo Y, Ward SM, Sanders KM, Yamanaka T, Fujino MA. Differential gene expression in the small intestines of wildtype and W/W(V) mice. *Neurogastroenterol Motil*. 2001;13(2):163–168. doi:10.1046/j.1365-2982.2001.00256.x
5. Müller M, Colcuc S, Drescher DG, et al. Murine genetic deficiency of neuronal nitric oxide synthase (nNOS(-/-)) and interstitial cells of Cajal (W/W(v)): implications for achalasia? *J Gastroenterol Hepatol*. 2014;29(10):1800–1807. doi:10.1111/jgh.12600
6. Lee JI, Park H, Kamm MA, Talbot IC. Decreased density of interstitial cells of Cajal and neuronal cells in patients with slow-transit constipation and acquired megacolon. *J Gastroenterol Hepatol*. 2005;20(8):1292–1298. doi:10.1111/j.1440-1746.2005.03809.x
7. Ward SM, Beckett EA, Wang X, Baker F, Khoyi M, Sanders KM. Interstitial cells of Cajal mediate cholinergic neurotransmission from enteric motor neurons. *J Neurosci*. 2000;20(4):1393–1403. doi:10.1523/JNEUROSCI.20-04-01393.2000
8. Huang Y, Mei F, Yu B, et al. Distribution of the interstitial Cajal-like cells in the gallbladder and extrahepatic biliary duct of the guinea-pig. *Acta Histochem*. 2009;111(2):157–165. doi:10.1016/j.acthis.2008.05.005
9. Liu Y, Fan Y, Wu S. Developments in research on interstitial Cajal-like cells in the biliary tract. *Expert Rev Gastroenterol Hepatol*. 2021;15(2):159–164. doi:10.1080/17474124.2021.1823214
10. Takao Y, Takaoka Y, Sugano A, et al. Shakuyaku-kanzo-to (Shao-Yao-Gan-Cao-Tang) as treatment of painful muscle cramps in patients with lumbar spinal stenosis and its minimum effective dose. *Kobe J Med Sci*. 2015;61(5):E132–E137.
11. Han K, Kwon O, Jung SY, et al. Jakyakgamcho-tang in the relief of delayed-onset muscle soreness in healthy adults: study protocol for a randomized, double-blind, placebo-controlled, crossover design clinical trial. *Trials*. 2020;21(1):211. doi:10.1186/s13063-020-4119-4
12. Chen M, Li F, Li XJ, et al. Clinical study of Shaoyao Gancao Decoction in treating II type Oddi sphincter dysfunction. *J Guangzhou Univ Tradition Chin Med*. 2021;38(4):681–686. Chinese.
13. Sui F, Zhou HY, Meng J, et al. A Chinese herbal decoction, Shaoyao-Gancao Tang, exerts analgesic effect by down-regulating the TRPV1 channel in a rat model of arthritic pain. *Am J Chin Med*. 2016;44(7):1363–1378. doi:10.1142/S0192415X16500762
14. Zhang XY, Cui GB, Ma KJ, et al. Sphincter of Oddi dysfunction in hypercholesterolemic rabbits. *Eur J Gastroenterol Hepatol*. 2008;20(3):202–208. doi:10.1097/MEG.0b013e3282f1d6ee
15. Wang F, Wang CM, Liu JD, Wang YT. Influence of paeoniflorin on intracellular calcium ion concentration in the sphincter of Oddi of hypercholesterolemic rabbits. *Genet Mol Res*. 2014;13(3):5001–5010. doi:10.4238/2014.July.4.15
16. Wei JG, Wang YC, Du F, Yu HJ. Dynamic and ultrastructural study of sphincter of Oddi in early-stage cholelithiasis in rabbits with hypercholesterolemia. *World J Gastroenterol*. 2000;6(1):102–106. doi:10.3748/wjg.v6.i1.102

17. Venu RP, Geenen JE. Diagnosis and treatment of diseases of the papilla. *Clin Gastroenterol*. 1986;15(2):439–456. doi:10.1016/S0300-5089(21)00696-9
18. Toouli J, Craig A. Sphincter of Oddi function and dysfunction. *Can J Gastroenterol*. 2000;14(5):411–419. doi:10.1155/2000/313601
19. Szilvássy Z, Nagy I, Madácsy L, et al. Beneficial effect of lovastatin on sphincter of Oddi dyskinesia in hypercholesterolemia and hypertriglyceridemia. *Am J Gastroenterol*. 1997;92(5):900–902.
20. Szilvassy Z, Sari R, Nemeth J, Nagy I, Csati S, Lonovics J. Improvement of nitrergic relaxation by farnesol of the sphincter of Oddi from hypercholesterolaemic rabbits. *Eur J Pharmacol*. 1998;353(1):75–78. doi:10.1016/S0014-2999(98)00449-X
21. Sarles JC, Delecourt P, Castello H, et al. Action of gastrointestinal hormones on the myoelectric activity of the sphincter of Oddi in living rabbit. *Regul Pept*. 1981;2(2):113–124. doi:10.1016/0167-0115(81)90005-7
22. Balunas MJ, Kinghorn AD. Drug discovery from medicinal plants. *Life Sci*. 2005;78:431–441. doi:10.1016/j.lfs.2005.09.012
23. Mishra BB, Tiwari VK. Natural products: an evolving role in future drug discovery. *Eur J Med Chem*. 2011;46:4769–4807.
24. Wang JX, Yang X, Zhang JJ, Zhou TT, Zhu YL, Wang LY. [Effects of Shaoyao Gancao decoction on contents of amino acids and expressions of receptors in brains of spastic paralysis rats]. *Zhongguo Zhong Yao Za Zhi*. 2016;41(6):1100–1106. Chinese.
25. Shao YY, Guo YT, Gao JP, et al. Shaoyao-Gancao decoction relieves visceral hyperalgesia in TNBS-induced postinflammatory irritable bowel syndrome via inactivating transient receptor potential vanilloid type 1 and reducing serotonin synthesis. *Evid Based Complement Alternat Med*. 2020;2020:7830280. doi:10.1155/2020/7830280
26. Hehir MP, Morrison JJ. Paeoniflorin, a novel heat-shock protein inducing compound, and human myometrial contractility in vitro. *J Obstet Gynaecol Res*. 2016;42:302–306. doi:10.1111/jog.12895
27. Sato Y, He JX, Nagai H, Tani T, Akao T. Isoliquiritigenin, one of the antispasmodic principles of Glycyrrhiza ularensis roots, acts in the lower part of intestine. *Biol Pharm Bull*. 2007;30(1):145–149. doi:10.1248/bpb.30.145
28. Liu B, Yang J, Wen Q, Li Y. Isoliquiritigenin, a flavonoid from licorice, relaxes guinea-pig tracheal smooth muscle in vitro and in vivo: role of cGMP/PKG pathway. *Eur J Pharmacol*. 2008;587(1–3):257–266. doi:10.1016/j.ejphar.2008.03.015
29. Wang F, Yang Y, Ji X, Tao X, Wang Y, Wang C. Effects of Paeoniflorin on the activity of muscle strips, intracellular calcium ion concentration and L-type voltage-sensitive calcium ion channels in the sphincter of Oddi of hypercholesterolemic rabbits. *Mol Med Rep*. 2019;19(6):5185–5194.
30. Song R, Wang CM, Xue WB, Ji XH. Preparation of Shaoyaoglycyrrhizae decoction containing serum and its effect on Ca~(2+) concentration in Oddi sphincter cells of hypercholesterolemic rabbits. *Chin Archiv Tradition Chin Med*. 2014;32:2612–2615.
31. Woods CM, Saccone GT. Neurohormonal regulation of the sphincter of Oddi. *Curr Gastroenterol Rep*. 2007;9(2):165–170. doi:10.1007/s11894-007-0012-5
32. Wang XY, Sanders KM, Ward SM. Intimate relationship between interstitial cells of cajal and enteric nerves in the guinea-pig small intestine. *Cell Tissue Res*. 1999;295(2):247–256. doi:10.1007/s004410051231
33. Nemeth L, Puri P. Three-dimensional morphology of c-Kit-positive cellular network and nitrergic innervation in the human gut. *Arch Pathol Lab Med*. 2001;125(7):899–904. doi:10.5858/2001-125-0899-TDMOCK
34. Huizinga JD, Ambrous K, Der-silaphet T. Co-operation between neural and myogenic mechanisms in the control of distension-induced peristalsis in the mouse small intestine. *J Physiol*. 1998;506(3):843–856. doi:10.1111/j.1469-7793.1998.843bv.x
35. Takayama I, Horiguchi K, Daigo Y, Mine T, Fujino MA, Ohno S. The interstitial cells of Cajal and a gastroenteric pacemaker system. *Arch Histol Cytol*. 2002;65(1):1–26. doi:10.1679/aohc.65.1
36. Ward SM, McLaren GJ, Sanders KM. Interstitial cells of Cajal in the deep muscular plexus mediate enteric motor neurotransmission in the mouse small intestine. *J Physiol*. 2006;573(1):147–159. doi:10.1113/jphysiol.2006.105189
37. Sanders KM, Ward SM. Nitric oxide and its role as a non-adrenergic, non-cholinergic inhibitory neurotransmitter in the gastrointestinal tract. *Br J Pharmacol*. 2019;176(2):212–227. doi:10.1111/bph.14459
38. Toma H, Nakamura K, Emson PC, Kawabuchi M. Immunohistochemical distribution of c-Kit-positive cells and nitric oxide synthase-positive nerves in the guinea-pig small intestine. *J Auton Nerv Syst*. 1999;75(2–3):93–99. doi:10.1016/S0165-1838(98)00167-2
39. Wang XY, Berezin I, Mikkelsen HB, et al. Pathology of interstitial cells of Cajal in relation to inflammation revealed by ultrastructure but not immunohistochemistry. *Am J Pathol*. 2002;160(4):1529–1540. doi:10.1016/S0002-9440(10)62579-5
40. Ivancheva C, Itzev D, Lolova I, Radomirov R. Contribution of nitric oxide and substance P to nonadrenergic, noncholinergic transmission in the guinea pig ileum. *Gen Pharmacol*. 1998;31(1):101–105. doi:10.1016/S0306-3623(97)00394-7
41. Iwasaki H, Kajimura M, Osawa S, et al. A deficiency of gastric interstitial cells of Cajal accompanied by decreased expression of neuronal nitric oxide synthase and substance P in patients with type 2 diabetes mellitus. *J Gastroenterol*. 2006;41(11):1076–1087. doi:10.1007/s00535-006-1909-8
42. Luo P, Liu D, Li C, He WX, Zhang CL, Chang MJ. Enteric glial cell activation protects enteric neurons from damage due to diabetes in part via the promotion of neurotrophic factor release. *Neurogastroenterol Motil*. 2018;30(10):e13368. doi:10.1111/nmo.13368
43. Lyford GL, He CL, Soffer E, et al. Pan-colonic decrease in interstitial cells of Cajal in patients with slow transit constipation. *Gut*. 2002;51(4):496–501. doi:10.1136/gut.51.4.496
44. Isozaki K, Hirota S, Miyagawa J, Taniguchi M, Shinomura Y, Matsuzawa Y. Deficiency of c-kit+ cells in patients with a myopathic form of chronic idiopathic intestinal pseudo-obstruction. *Am J Gastroenterol*. 1997;92(2):332–334.
45. He CL, Soffer EE, Ferris CD, Walsh RM, Szurszewski JH, Farrugia G. Loss of interstitial cells of cajal and inhibitory innervation in insulin-dependent diabetes. *Gastroenterology*. 2001;121(2):427–434. doi:10.1053/gast.2001.26264
46. Kenny SE, Connell MG, Rintala RJ, Vaillant C, Edgar DH, Lloyd DA. Abnormal colonic interstitial cells of Cajal in children with anorectal malformations. *J Pediatr Surg*. 1998;33(1):130–132. doi:10.1016/S0022-3468(98)90379-7
47. Estaquier J, Vallette F, Vayssiere JL, Mignotte B. The mitochondrial pathways of apoptosis. *Adv Exp Med Biol*. 2012;942:157–183.
48. Suen DF, Norris KL, Youle RJ. Mitochondrial dynamics and apoptosis. *Genes Dev*. 2008;22(12):1577–1590. doi:10.1101/gad.1658508
49. Idriss HT, Naismith JH. TNF alpha and the TNF receptor superfamily: structure-function relationship(s). *Microsc Res Tech*. 2000;50(3):184–195. doi:10.1002/1097-0029(20000801)50:3<184::AID-JEMT2>3.0.CO;2-H

50. Torihashi S, Ward SM, Sanders KM. Development of c-Kit-positive cells and the onset of electrical rhythmicity in murine small intestine. *Gastroenterology*. 1997;112(1):144–155. doi:10.1016/S0016-5085(97)70229-4
51. Tong W, Jia H, Zhang L, Li C, Ridolfi TJ, Liu B. Exogenous stem cell factor improves interstitial cells of Cajal restoration after blockade of c-kit signaling pathway. *Scand J Gastroenterol*. 2010;45(7–8):844–851. doi:10.3109/00365521003782371
52. Chen J, Du L, Xiao YT, Cai W. Disruption of interstitial cells of Cajal networks after massive small bowel resection. *World J Gastroenterol*. 2013;19(22):3415–3422. doi:10.3748/wjg.v19.i22.3415
53. Archana M, Bastian YTL, Kumaraswamy KL, Yogesh TL. Various methods available for detection of apoptotic cells–a review. *Indian J Cancer*. 2013;50(3):274–283. doi:10.4103/0019-509X.118720